Engineering Solid Mechanics 11 (2023) 125-134

Contents lists available at GrowingScience

Engineering Solid Mechanics

homepage: www.GrowingScience.com/esm

A micromechanical study on the correlation of the microstructure and failure mechanism of dual-phase steels under tension

M.S. Mohsenzadeh[a*]

[a]*Department of Materials and Metallurgical Engineering, University of Gonabad, Gonabad, Iran*

ARTICLEINFO

Article history:
Received 20 September 2022
Accepted 12 January 2023
Available online
12 January 2023

Keywords:
Dual-phase steel
Failure mechanism
Microstructure-based modeling
Martensite particle size
Martensite volume fraction

ABSTRACT

In this study, the influence of the volume fraction of the martensite phase as well as the size of the martensite particles on the mechanism of particle fracture in dual-phase steel were examined. A combined continuum/dislocation based approach was used in order to model the average stress in the martensite particles. It was found that the model predictions are in accordance with the experimental results. For the same volume fraction of the martensite particles, the model predicts an increase of the internal stress and the average stress in the martensite particles with increasing the particles size. Since the fracture strength of the martensite depends on its volume fraction, the particle size has no effect on the mechanism of particle fracture. Increasing the volume fraction of the martensite particles results in the enhancement of the internal stress in the martensite particles. However, it has a slight influence on the average stress in the particles. Nevertheless, because of decreasing the fracture strength of martensite with increasing its volume fraction, this parameter has a main role in the occurrence of the particle fracture mechanism.

1. Introduction

Dual-phasesteels (DPS) with a microstructure including soft ferrite matrix and typically5 to 30% hard martensite islands, have characteristic properties such as highstrength and work hardening rate as well as good ductility. The mechanical propertiesand the failure mechanisms of dual-phase steels are controlled by theirmicrostructures. Therefore, the volume fraction, morphology, size anddistribution of the constituent phases have a significant effect on themechanical properties and failure mechanisms of dual-phase steels. Knowingabout the particular effect of the microstructure on the mechanical propertiesand also failure mechanisms of such materials is essential to adjust theirproperties for industrial applications. Toinvestigate the fracture behavior of dual-phase steels, the ductile failure modelwhich is done by the mechanism of void nucleation, void growth and voidcoalescence, has been used in several studies (Balliger,1982; de Geus, Peerlings, & Geers, 2016; Gladman, 1997; Hosseini-Toudeshky, Anbarlooie, & Kadkhodapour, 2015; Kadkhodapour, Butz, & Rad, 2011; Kang, Ososkov, Embury, & Wilkinson, 2007; Koo& Thomas, 1977; Maire,Bouaziz, Di Michiel, & Verdu, 2008; Rashid,1977; Rashid & Cprek, 1978; Saeidi, Ashrafizadeh, Niroumand, Forouzan, & Barlat,2014; Steinbrunner, Matlock, & Krauss,1988; Sun & Pugh, 2002; Wuet al., 2017). Manyattempts have been made to investigate the mechanism of void nucleation in thismodel. In a study investigating the fracture behavior of DP steel containinglath martensite, it was found that the ferrite-martensite interface decohesionwas the most prevalent mechanism of void nucleation and growth (Kang & Kwon, 1987). Themechanism of martensite particle cracking was not observed for martensitevolume fraction from 15% to 20% (Szewczyk& Gurland, 1982). Ahmed et al. (2000) showed that themechanism of void nucleation was ferrite-martensite interface decohesion at lowto intermediate volume fraction of martensite, while void nucleation was due tomartensite cracking and decohesion at the ferrite-ferrite interfaces at highvolume fraction, above 32%. The results of a study conducted on theinvestigation of the failure mechanism of a dual-phase steel, showed that thevoid nucleation occurred by the ferrite grain boundary decohesion in

* Corresponding author. Tel. +985157229701
E-mail addresses: mohsenzadeh@gonabad.ac.ir (M.S. Mohsenzadeh)

ISSN 2291-8752 (Online) - ISSN 2291-8744 (Print)

doi: 10.5267/j.esm.2023.1.003

theneighborhood of martensite grains as well as between closely situatedmartensite grains (Kadkhodapour, Butz, & Rad, 2011). Several models havebeen developed to show the mechanism of failure in dual-phase steels (deGeus et al., 2016; Hosseini-Toudeshky et al., 2015; Kadkhodapour, Butz, & Rad, 2011; Paul, 2012, 2013; Saeidi et al., 2014; Wuet al., 2017).

Modellingof the general failure mechanism of DPS does not appear to be applicable.Instead, the main failure mechanism based on the relevant microstructuralparameters of DPS should be taken into account (Kadkhodapour,Butz, & Rad, 2011). A simple shear lagmodel has been used for modelling the fracture of lath shaped precipitatesin an aluminum alloy (AA6111) (Proudhon, Poole, Wang, & Brechet,2008). Usingthis model, a condition for the fracture has been derived by assuming that theload is transferred to the reinforcement via interfacial shear stresses.Conventionally, the shear lag model has been utilized for modelling the fractureof reasonably long fibers. This model is not applicable for compositesincluding whiskers. Because the model leads to an aspect ratio greater thanthose typically retained in the real whisker composites (Clyne & Withers, 1995). Besides,relaxation processes that reduce the fiber stress at a given plastic strain arenot considered in this model.The probability of the fracture of thereinforcement can be examined by considering the reinforcement stresses thatoccur in the composite (Clyne &Withers, 1995). In this study, by adopting a composite view ofdual-phase steel, a model based on physical properties including plasticrelaxation has been proposed to predict the evolution of the average stress in themartensite particles as a function of the applied strain. Knowing themicrostructural features like the particle's radius and volume fraction makes itpossible to accurately estimate the average stress of the martensite particles.The model was used to clarify the failure mechanisms in dual-phase steelspecimens and find out about the influence of particle size and volume fractionon the mechanism of martensite particle fracture. The obtained results could begeneralized to the particulate composites. To the best of the author'sknowledge, the present study is the first of its kind that examines the influenceof particle size on the mechanism of martensite particle fracture throughmicrostructure-based modelling. The influence of particle size on the mechanismof martensite particle fracture could not be examined through continuum modelslike finite element models.

2. Experimental procedure

The present study used a sheet of plain carbon steel 4.6 mm in thick. Table 1 shows the chemical composition of the steel used in this study. Samples with the size of 100 mm × 20 mm were cut from the sheet and were then austenized at 1000 °C for 30 min. The samples were then quenched in an ice brine solution. The obtained martensitic structures were tempered at 650 °C for 1 hr, and then a laboratory rolling mill (the roll diameter 57cm and the peripheral speed of 40 rpm) was used to cold roll the martensitic structures by 80 pct reduction in thickness. The cold rolled samples were tempered for another 2 hr at 650 °C. This heat treatment cycle formed a microstructure of cementite particles which were uniformly dispersed in a ferrite matrix. The ferrite-cementite microstructure samples were used for intercritical annealing at 740 °C for 1 and 15 min followed by quenching into an ice brine solution.

To analyze the fracture mechanisms of samples, tensile tests were used. Specimens with the gauge length of 25 mm were prepared according to ASTM-E8 standard and loaded with Zwick Z250 universal tensile test machine with the strain rate of 0.002 s^{-1}. Fractured specimens were sectioned along their mid-plane, parallel to the tensile axis, and the region adjacent to the fracture surface was observed by scanning electron microscopy (SEM) (Leo 1450VP). Besides, the microstructure of the undeformed region of the fractured specimens was examined using Olympus-BX60M optical microscope. Specimen preparations for observing microstructures included mounting, mechanically grounding and polishing, and then etching using 3 pct Nital solution. Clemex image analysis software was used to measure the size of martensite islands and also volume fraction of martensite phase. Undeformed regions of the steel specimens were analyzed by taking at least ten different images. Clemex image analysis software was also used to measure ferrite grain size based on the linear intercept approach.

Table 1. The chemical composition of the low-carbon steel sheet (in weight percent).

C	Mn	Si	P	S	Cr	Ni	Al	Fe
0.165	1.15	0.411	0.018	0.01	0.035	0.066	0.042	Bal.

3. Results and Discussion

3.1. Steel microstructures

The steel microstructures obtained from the intercritical annealing treatment at 740 °C for 1 and 15 min are shown in **Fig. 1a** and **Fig. 1b**, respectively. As can be seen, microstructures consist of ferrite-cementite-martensite (**Fig. 1a**) and ferrite-martensite (**Fig. 1b**) were produced. Table 2 shows the nomenclatures of the steel samples and also the quantitative metallography results which consist of the volume fractions of martensite phase (f_M), the size of martensite islands (d_M) and the ferrite grain size (d_f).

Considering the results, there are 1.2% cementite particles in the microstructure of the specimen F-13M. According to the literature, the presence of cementite particles does not influence the principal fracture mechanism of dual-phase steels (Kadkhodapour, Butz, & Rad, 2011). Besides, the obtained results in this study indicate that the cementite particles have no role in the failure mechanism of steel F-13M. Therefore, the effect of the martensite phase in the fracture mechanism could be examined.

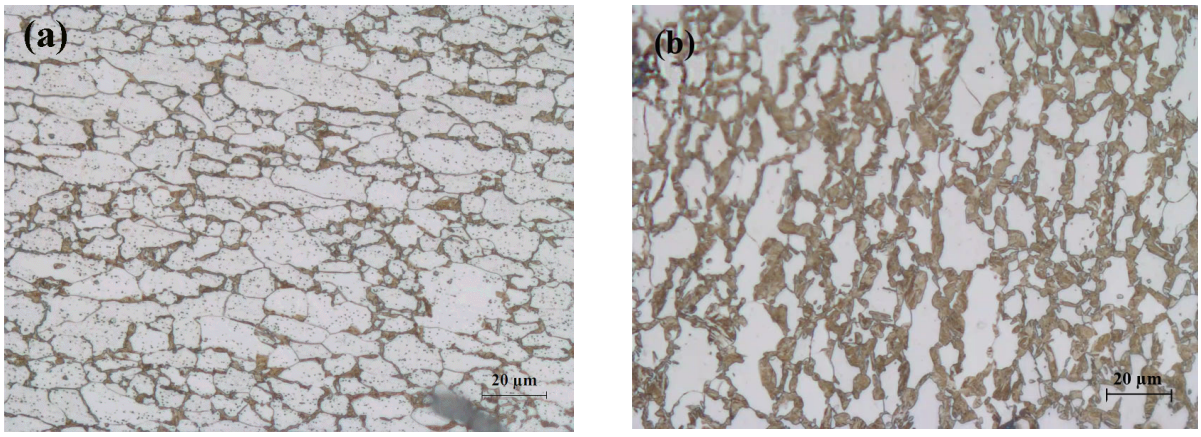

Fig. 1. Optical micrographs representing the microstructures of the steel samples after intercritical annealing at 740 °C for: (a) 1 min, and (b) 15 min

Table 2. Martensite volume fraction (f_M), martensite island size (d_M), and the ferrite grain size (d_f) in the steel microstructures.

Nomenclature	Microstructure	f_M (%)	d_M (µm)	d_f (µm)
F-13M	Ferrite+cementite+martensite	13	2.25	10
F-40M	Ferrite+martensite	40	4.15	10

3.2. Failure mechanisms

SEM micrograph of the necked region of the fractured specimen F-13M is illustrated in **Fig. 2.** The tensile load direction in this Figure is vertical. The micrograph shows in detail the microstructure and void formation of the specimen F-13M. Nearly spherical voids are nucleated in the immediate vicinity of surfaces of martensite particles normal to the load (indicated by arrows in the **Fig. 2**). This type of void formation mechanism is caused by a locally high hydrostatic stress (Clyne & Withers, 1995; Kadkhodapour, Butz, & Rad, 2011). Because of the high strength of ferrite-martensite interface (Lee, Hwang, Lee, Lee, & Kim, 2004), the mechanism of ferrite-martensite interface debonding could not occur (Clyne & Withers, 1995). Thus, the voids are formed within the matrix where the hydrostatic component of the local stresses is the greatest, e.g. near the martensite surface normal to the load. In these regions, a critical hydrostatic stress, characteristic of the ferrite matrix, is exceeded. The microstructure and void formation of the specimen F-40M are shown in **Fig. 3**. Another type of the mechanism of void formation can be observed in the Figure. In this specimen, the fracture of martensite particles took place, and the deformation of the surrounding ferrite matrix led to the formation of spherical voids (indicated by arrows in the **Fig. 3**). During deformation of the specimen, the load is passed on the martensite particles because of the deformation mismatch between ferrite matrix and martensite particles. When the stress in the martensite particles exceeds the fracture strength of martensite, the fracture of martensite particles occurs.

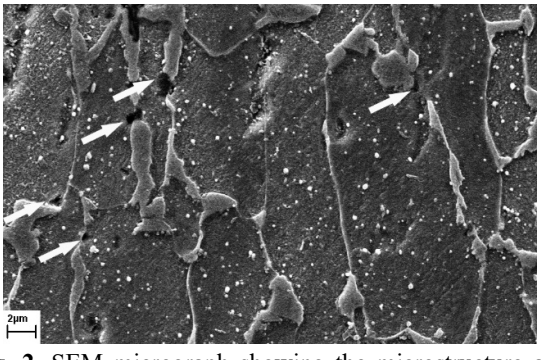

Fig. 2. SEM micrograph showing the microstructure and void formation of the specimen F-13M taken from the necked region of the fractured tensile sample

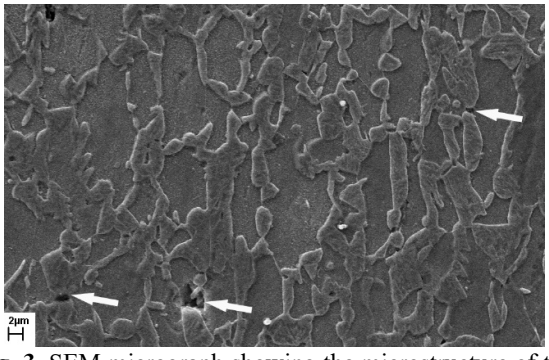

Fig. 3. SEM micrograph showing the microstructure of the specimen F-40M taken from the necked region of the fractured tensile sample

3.3. Proposed explanation of the failure mechanism through modeling

In order to model the internal stress in the martensite particles, Eshelby approach was used. According to this approach, the load transfer is estimated using the misfit strain. The misfit strain is calculated from the difference between the natural shape

of the reinforcement and the natural shape of the hole in which it is located (Clyne & Withers, 1995). The internal stress in the martensite particles $\langle\sigma\rangle_I$ can be calculated as (Brown & Stobbs, 1971; Clyne & Withers, 1995):

$$\langle\sigma\rangle_I = (1-f)E_p\varepsilon_p^* \tag{1}$$

where f is martensite volume fraction, E_p stands for the Young's modulus of the martensite particle, and ε_p^* stands for the unrelaxed plastic strain. A large misfit strain could be created even at small plastic strain of the matrix. This results in a strong load transfer to the reinforcement which may not be sustainable. Under these conditions, various plastic relaxation processes will occur to reduce the shape misfit. As a result, the internal stress in the reinforcement decreases. The unrelaxed plastic strain (ε_p^*) is the net misfit strain after plastic relaxation (Clyne & Withers, 1995). A physically-based expression was used for the assessment of ε_p^* which deals with the effect of particle size (Brown & Stobbs, 1971). As a result, aspects of both continuum and dislocation based approaches are incorporated in the model. ε_p^* was estimated from the following equation (Brown & Stobbs, 1971):

$$\varepsilon_p^* = \frac{nb}{2rM} \tag{2}$$

In which the number of Orowan dislocation loops stored around a particle is shown by n, the burgers vector is shown by b, the average radius of the martensite particles is shown by r, and the average Taylor factor being 3.06 for the case of polycrystalline metals with cubic crystal lattice is shown by M (Delincé et al., 2007). The rate of the storage of Orowan dislocation loops as a function of the plastic strain in the matrix is expressed as follows (Mohsenzadeh & Mazinani, 2017; Proudhon et al., 2008):

$$\frac{\partial n}{\partial \varepsilon_p} = M\frac{2r\beta}{b}\left(1-\frac{n}{n^*}\right) \tag{3}$$

In this equation, the maximum number of the stored dislocation loops is shown by n^*, the plastic strain in the ferrite matrix is shown by ε_p, and the constant coefficient less than unity is shown by β. n^* was determined by fitting the theoretical stress-strain curve to the experimental stress-strain curve obtained from the tensile test. Details of the modeling of the deformation behavior of dual-phase steel have been explained in the previous study (Mohsenzadeh & Mazinani, 2017). Once n^* is specified, ε_p^* can be calculated. According to the above equation, the rate by which n increases by the plastic strain, ε_p, is decreased. Therefore, the number of dislocation loops stored around a particle approach an upper limit, n^*. It has been demonstrated that this equation appropriately incorporates the plastic relaxation into the model (Mohsenzadeh & Mazinani, 2017). Finally, the average stress, σ_{ave}, in the martensite particles can be obtained as (Clyne & Withers, 1995):

$$\sigma_{ave} = \sigma_A + \langle\sigma\rangle_I \tag{4}$$

where σ_A is the flow stress. If the stress that martensite particles undergo, i.e. the average stress, is greater than the flow stress of the martensite phase, particle fracture will occur. In order to illustrate the strain hardening behavior of the martensite phase in the DP steel specimen, an empirical model was used. The correctness of the propositions based on the model formulation was demonstrated to be satisfactory (Kadkhodapour, Butz, Ziaei-Rad, & Schmauder, 2011; Vajragupta et al., 2012). According to this model, the stress-strain relation of the martensite phase is shown in the following Equation (Rodriguez & Gutiérrez, 2003):

$$\sigma = \sigma_o + \Delta\sigma + \alpha M\mu\sqrt{b}\sqrt{\frac{1-\exp\left(-Mk\varepsilon_{p,M}\right)}{kL}} \tag{5}$$

$$\sigma_o = 77 + 80\%Mn + 750\%P + 60\%Si + 80\%Cu + 45\%Ni + 60\%Cr + 11\%Mo + 5000N_{ss} \tag{6}$$

$$\Delta\sigma = 3065\%C - 161 \tag{7}$$

In this equation, the constant is shown by α (α = 0.33), the shear modulus is shown by μ (μ=80 GPa), the dislocation mean free path is shown by L, the recovery rate is shown by k, the plastic strain in the martensite phase being equal to the unrelaxed

plastic strain is shown by $\varepsilon_{p,M}$, and the additional strengthening due to the carbon in solution is shown by $\Delta\sigma$. The energy dispersive X-ray analyzer (EDS) was used to measure the carbon concentration in the martensite islands and 0.502 wt% and 0.4 wt% were obtained for specimens F-13M and F-40M, respectively. σ_o deals with the effect of Peierl's stress and solid solution strengthening. $\Delta\sigma$ and σ_o are presented in Eq. (6) and Eq. (7), respectively. The model used the following parameters shown in Table 3.

Table 3. The parameters and their values used in the model.

Parameter	Symbol	Value	Origin
Taylor constant	α	0.33	Ref. (Kadkhodapour, Butz, Ziaei-Rad, et al., 2011)
Taylor factor	M	3.06	Ref. (Delincé et al., 2007)
Burgers vector	b	0.26 nm	Ref. (Delincé et al., 2007)
The shear modulus of martensite	μ	80 GPa	Ref. (Kadkhodapour, Butz, Ziaei-Rad, et al., 2011)
The Young's modulus of martensite	E_p	210 GPa	Ref. (Hertzberg & Hauser, 1977)
The average radius of the martensite particles	r	1.12 μm (specimen F-13M) 2.07 μm (specimen F-40M)	Metallography
Martensite volume fraction	f	13% (specimen F-13M) 40% (specimen F-40M)	Metallography
Maximum number of the stored dislocation loops around a particle	n^*	245 (specimen F-13M) 350 (specimen F-40M)	Fitting parameter
The dislocation mean free path in the martensite	L	3.8×10^{-8} m	Ref. (Kadkhodapour, Butz, Ziaei-Rad, et al., 2011)
The recovery rate	k	41	Ref. (Kadkhodapour, Butz, Ziaei-Rad, et al., 2011)

Fig. 4 shows the variation of ε_p^* with the applied plastic strain $\left(\bar{\varepsilon}_p\right)$ for martensite particles in the specimens F-13 and F-40. Considering the specimen F-40M, **Fig.** 4 indicates that the magnitude of ε_p^* is greater for the coarser martensite particles. With respect to Eq. (2), ε_p^* is influenced by both the particle radius, *r*, and *n*. Increasing *r* decreases ε_p^*, and increasing n increases ε_p^*. Because of larger *r* and greater *n**, the rate of dislocation loop storage around martensite particles in the specimen F-40M is relatively greater than the specimen F-13M. Based on the results of **Fig. 4**, it is clear that the effect of *n* on ε_p^* is more predominant. In **Fig. 5**, the internal stress in the martensite particles, $\langle\sigma\rangle_I$, is plotted as a function of the applied plastic strain $\left(\bar{\varepsilon}_p\right)$ for the specimen F-13M and the specimen F-40M. As Figure 4 shows, $\langle\sigma\rangle_I$ for martensite particles in the specimen F-13M is substantially greater than the specimen F-40M. Only at the low plastic strains, $\langle\sigma\rangle_I$ for martensite particles in the specimen F-13M is slightly lower. Both ε_p^* and volume fraction of martensite (*f*) affect the internal stress. As the misfit strain $\left(\varepsilon_p^*\right)$ for martensite particles in the specimen F-40M is greater than that in the specimen F-13M, it might be speculated that the internal stress for martensite particles in the former to be greater than the latter. However, martensite particles are indeed less highly stressed when they involve more of the volume (Clyne & Withers, 1995). As a result, a smaller internal stress is created in the martensite particles of the specimen F-13M than in the specimen F-40M.

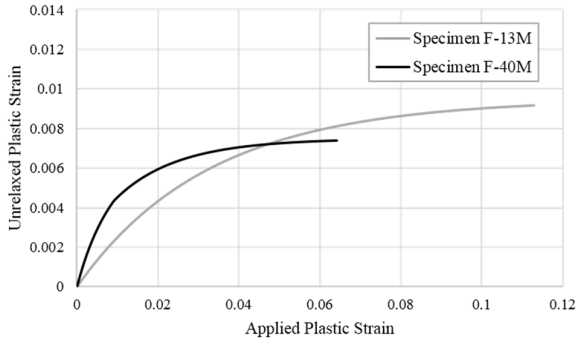

Fig. 4. The unrelaxed plastic strain, ε_p^*, plotted versus the applied plastic strain $\left(\bar{\varepsilon}_p\right)$ for martensite particles in the specimens F-13 and F-40

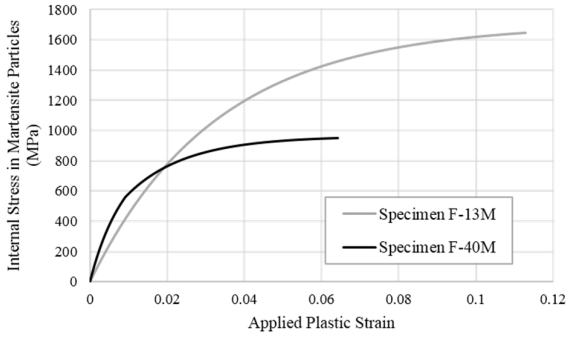

Fig. 5. The internal stress in the martensite particles, $\langle\sigma\rangle_I$, plotted versus the applied plastic strain $\left(\bar{\varepsilon}_p\right)$ for the specimens F-13 and F-40.

The average stress (σ_{ave}) for the martensite particles in the specimen F-40M is greater in the specimen F-13M (**Fig. 6**). Load transfer to the martensite particles is more effective in the specimen F-40M because martensite particles are coarser. Besides, this specimen has a higher volume fraction of martensite. Consequently, the kinematic work hardening and thereby the flow stress of the specimen F-40M are greater in comparison to the specimen F-13M (Mohsenzadeh & Mazinani, 2017). The higher flow stress in the specimen F-40M than the specimen F-13M is to the extent that it compensates for the lower internal stress in the martensite particles of the specimen F-40M, and finally the average stress in the martensite particles of the specimen F-40M is much higher compared to the specimen F-13M. The specimen F-13M continues to deform at the strains greater than the fracture strain of specimen F-40M, and the average stress in the martensite particles of this specimen increases to the values higher than that of the specimen F-40M.

The calculated strain hardening behavior of the martensite phase for each specimen is shown in **Fig. 6**. As can be observed, the flow stress of martensite in the specimen F-40M is lower than that in the specimen F-13M. The value of the flow stress is controlled by the carbon content in the martensite. The higher the volume fraction of martensite, the lower its carbon content and the lower its flow stress for a given strain. In order to examine the probability of the fracture of martensite particles, one must compare the average stress and the flow stress of martensite during straining. In the specimen F-40M, the average stress of martensite at the final stages of straining becomes higher than its flow stress, while in the specimen F-13M, the average stress of martensite is always less than its flow stress. Consequently, fracture of martensite particles occurred in the specimen F-40M.

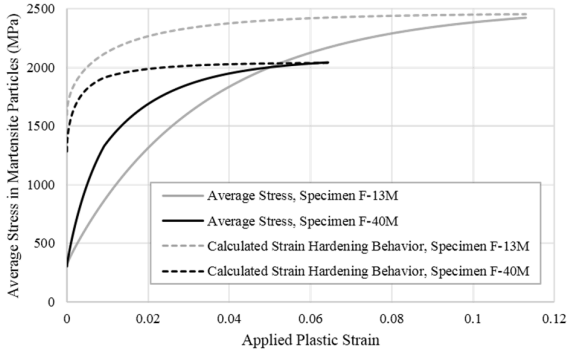

Fig. 6. The average stress in the martensite particles, σ_{ave}, as well as the calculated strain hardening behavior of the martensite phase plotted versus the applied plastic strain $\left(\bar{\varepsilon}_p\right)$ for the specimens F-13 and F-40.

The developed model was used to draw conclusions about the influence of particle size and volume fraction on the fracture of martensite particles. The variation of the internal stress in the martensite particles, $\langle\sigma\rangle_I$, as a function of the plastic strain applied to the steel, $\bar{\varepsilon}_p$, for different particle sizes and the same volume fractions are illustrated in Figures 7a and 7b. As these figures illustrate, $\langle\sigma\rangle_I$ for coarser particles (4.15 μm in diameter) is greater than that of finer particles (2.25 μm in

diameter), and only at the final strains decreases to the smaller values. According to the Eq. (1), $\langle\sigma\rangle_I$ only depends on ε_p^* with respect to the same volume fraction of second phase particles. In comparison to fine particles, coarse particles result in a higher $\langle\sigma\rangle_I$ due to the greater value of ε_p^*.

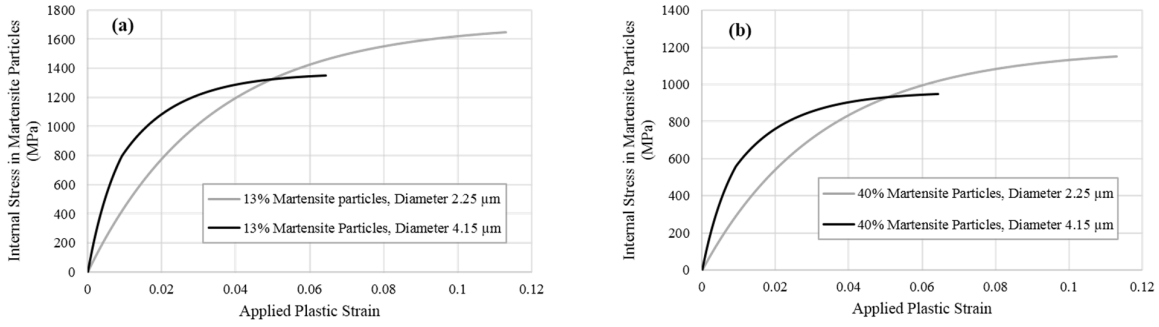

Fig. 7. The internal stress in the martensite particles, $\langle\sigma\rangle_I$, as a function of $\bar{\varepsilon}_p$ for the same volume fractions of martensite particles with diameters 2.25 µm and 4.15 µm, a) 13%, b) 40%.

Fig. 8 illustrates the variation of the average stress in the martensite particles as a function of the plastic strain applied to the steel for different particle sizes and the same volume fractions. As the results in **Fig. 7** show, except for the final strains, σ_{ave} for coarser particles (4.15 µm in diameter) is greater than that of finer particles (2.25 µm in diameter). According to the Equation 4, σ_{ave} is dependent on $\langle\sigma\rangle_I$ and the flow stress. As mentioned previously, $\langle\sigma\rangle_I$ in the coarser particles is greater than the finer particles. Besides, because of the more effective load transfer to the coarser particles, the flow stress of the specimen consisting of coarser martensite particles is greater than the specimen consisting of finer martensite particles (Mohsenzadeh & Mazinani, 2017). Consequently, the average stress increases along with increasing particle size.

The fracture strength of martensite depends only on its volume fraction and is independent of its particle size (Delincé et al., 2007). As Figure 8 shows, at the low volume fraction of martensite (13%), its fracture strength is higher than the average stress, and fracture does not occur in the martensite particles of any size. As the volume fraction of martensite increases, its carbon content and the fracture strength decrease. At higher volume fractions (40%), the fracture strength of martensite reduces to less than the average stress, and fracture occurs in the martensite particles of any size. Therefore, it might be argued that in the constant volume fraction of martensite, the particle size of martensite has no effect on the mechanism of martensite particle fracture because the fracture strength of martensite does not depend on its particle size.

In the case of composites, the fracture strength of particles of any size is the same. Because of containing a sufficiently large flaw, the fracture strength of coarse particles is somewhat reduced (Clyne & Withers, 1995). In general, it can be said that coarse particles in the composites are more likely to fracture because they have greater average stress and smaller fracture strength compared to fine particles.

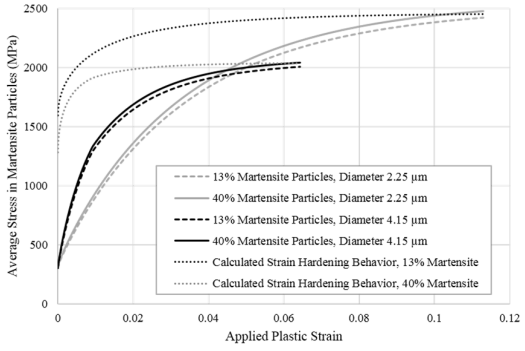

Fig. 8. The average stress in the martensite particles, σ_{ave}, plotted versus $\bar{\varepsilon}_p$ for volume fractions 13% and 40%, and martensite particle diameters 2.25 µm and 4.15 µm.

The variations of $\langle\sigma\rangle_I$ with $\bar{\varepsilon}_p$ for different volume fractions and the same martensite particle sizes are shown in Figure 9a and b. As can be clearly observed, the internal stress in the martensite particles decreases with increasing the volume fraction of martensite. For a given particle size, the unrelaxed plastic strain is constant, and the internal stress depends only on the volume fraction. As the particle volume fraction increases, $\langle\sigma\rangle_I$ decreases because the individual particles are actually less greatly stressed when they involve more of the volume (Clyne & Withers, 1995).

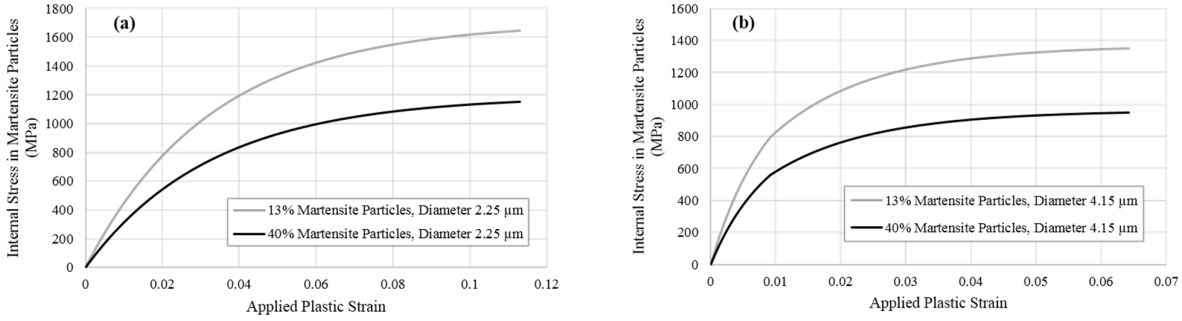

Fig. 9. The internal stress in the martensite particles, $\langle\sigma\rangle_I$, plotted versus $\bar{\varepsilon}_p$ for the same martensite particle size and volume fractions 13% and 40%, a) particle diameter 2.25 μm, b) particle diameter 4.15 μm.

According to **Fig. 8**, the average stress increases only slightly with increasing particle volume fraction. Although the kinematic work hardening and thereby the flow stress increase as the volume fraction of martensite particles increases, the internal stress decreases. Therefore, increasing the particle volume fraction has little effect on the average stress. On the other hand, as the volume fraction of martensite increases, its fracture strength decreases. Consequently, regardless of the particle size, the fracture of martensite particles occurs with increasing martensite volume fraction.

In the case of composites, the fracture strength changes only by changing the particle size. Therefore, it might be true to say that changing the volume fraction of particles has no effect on the occurrence of the mechanism of particle fracture.

4. Conclusion

The present study used a microstructure-based model to investigate the effect of martensite particle size and volume fraction on the mechanism of martensite particle fracture in dual-phase steels. For this purpose, a modelling approach which incorporates aspects of both continuum and dislocation based approaches has been developed to predict the evolution of the average stress in the martensite particles as a function of the applied strain. The model considers the effect of particle size on the average stress, and includes plastic relaxation.

The model predicts an increase of the internal stress in the martensite particles, $\langle\sigma\rangle_I$, with increasing the particle size, which is due to the increase of the unrelaxed plastic strain (the net misfit strain), ε_p^*. Average stress in the martensite particles, σ_{ave}, also increases with increasing particle size, which is attributed to the increase of the internal stress in the martensite particles as well as the specimen flow stress. Only at the final strains, $\langle\sigma\rangle_I$ and σ_{ave} for coarser particles decreases to the smaller values compared to the finer particles. The results of the model prove that the particle size has no effect on the particle fracture if the volume fraction of martensite is constant. This is because the fracture strength of martensite is dependent on its volume fraction, and is constant at a constant volume fraction of martensite.

Based on the modeling results, as the volume fraction of martensite particles increases, $\langle\sigma\rangle_I$ decreases because the individual particles are actually less greatly stressed when they involve more of the volume. Increasing the volume fraction of martensite particles causes a slight increase of σ_{ave}. This is due to the increase of the sample flow stress and the decrease of $\langle\sigma\rangle_I$ with increasing particle volume fraction. Since the fracture strength of martensite decreases with increasing its volume fraction, regardless of the particle size, the mechanism of particle fracture occurs as the martensite volume fraction increases.

The obtained results could be generalized to the particulate composites. In general, it can be said that coarse particles in the composites are more likely to fracture because they have greater σ_{ave} and smaller fracture strength compared to fine particles. Besides, because the fracture strength is not dependent on the particle volume fraction, and the σ_{ave} changes slightly with the change of the particle volume fraction, changing the volume fraction of particles has no effect on the occurrence of the mechanism of particle fracture.

Data availability statements

The datasets generated during and/or analyzed during the current study are available from the corresponding author on reasonable request.

References

Ahmad, E., Manzoor, T., Ali, K. L., & Akhter, J. (2000). Effect of microvoid formation on the tensile properties of dual-phase steel. *Journal of materials engineering and performance, 9*(3), 306-310.

Balliger, N. (1982). Advances in the physical metallurgy and applications of steels. *The Metals Society*, 73-83.

Brown, L., & Stobbs, W. (1971). The work hardening of copper-silica, parts I and IT. *Phil. Mag, 23*, 1187-1199.

Clyne, T., & Withers, P. (1995). *An introduction to metal matrix composites*: Cambridge university press.

de Geus, T., Peerlings, R., & Geers, M. (2016). Competing damage mechanisms in a two-phase microstructure: How microstructure and loading conditions determine the onset of fracture. *International Journal of Solids and Structures, 97*, 687-698.

Delincé, M., Bréchet, Y., Embury, J. D., Geers, M. G. D., Jacques, P. J., & Pardoen, T. (2007). Structure–property optimization of ultrafine-grained dual-phase steels using a microstructure-based strain hardening model. *Acta Materialia, 55*(7), 2337-2350. doi: https://doi.org/10.1016/j.actamat.2006.11.029

Gladman, T. (1997). The Physical Metallurgy of Microalloyed Steels, London, Inst: Materials.

Hertzberg, R. W., & Hauser, F. E. (1977). Deformation and fracture mechanics of engineering materials.

Hosseini-Toudeshky, H., Anbarlooie, B., & Kadkhodapour, J. (2015). Micromechanics stress–strain behavior prediction of dual phase steel considering plasticity and grain boundaries debonding. *Materials & Design, 68*, 167-176.

Kadkhodapour, J., Butz, A., & Rad, S. Z. (2011). Mechanisms of void formation during tensile testing in a commercial, dual-phase steel. *Acta Materialia, 59*(7), 2575-2588.

Kadkhodapour, J., Butz, A., Ziaei-Rad, S., & Schmauder, S. (2011). A micro mechanical study on failure initiation of dual phase steels under tension using single crystal plasticity model. *International Journal of Plasticity, 27*(7), 1103-1125.

Kang, J., Ososkov, Y., Embury, J. D., & Wilkinson, D. S. (2007). Digital image correlation studies for microscopic strain distribution and damage in dual phase steels. *Scripta Materialia, 56*(11), 999-1002.

Kang, S.-M., & Kwon, H. (1987). Fracture behavior of intercritically treated complex structure in medium-Carbon 6Ni steel. *Metallurgical transactions A, 18*(9), 1587-1592.

Koo, J., & Thomas, G. (1977). Formable HSLA and Dual-Phase Steels, ed. by AT Davenport. *AIME, New York, 40*.

Lee, H. S., Hwang, B., Lee, S., Lee, C. G., & Kim, S.-J. (2004). Effects of martensite morphology and tempering on dynamic deformation behavior of dual-phase steels. *Metallurgical and Materials Transactions A, 35*(8), 2371-2382.

Maire, E., Bouaziz, O., Di Michiel, M., & Verdu, C. (2008). Initiation and growth of damage in a dual-phase steel observed by X-ray microtomography. *Acta Materialia, 56*(18), 4954-4964.

Mohsenzadeh, M. S., & Mazinani, M. (2017). The effect of particles size on work hardening behavior of a low carbon steel with a composite-type microstructure. *Materials Science and Engineering: A, 702*, 113-124.

Paul, S. K. (2012). Micromechanics based modeling of Dual Phase steels: Prediction of ductility and failure modes. *Computational Materials Science, 56*, 34-42.

Paul, S. K. (2013). Effect of martensite volume fraction on stress triaxiality and deformation behavior of dual phase steel. *Materials & Design, 50*, 782-789.

Proudhon, H., Poole, W. J., Wang, X., & Brechet, Y. (2008). The role of internal stresses on the plastic deformation of the Al–Mg–Si–Cu alloy AA6111. *Philosophical Magazine, 88*(5), 621-640.

Rashid, M. (1977). Paper 760206, Soc. *Auto. Eng. Cong, Detroit*, 938-949.

Rashid, M., & Cprek, E. (1978). Relationship between microstructure and formability in two high-strength, low-alloy steels. *ASTM special technical publication, 647*, 174-190.

Rodriguez, R., & Gutiérrez, I. (2003). *Unified formulation to predict the tensile curves of steels with different microstructures.* Paper presented at the Materials Science Forum.

Saeidi, N., Ashrafizadeh, F., Niroumand, B., Forouzan, M., & Barlat, F. (2014). Damage mechanism and modeling of void nucleation process in a ferrite–martensite dual phase steel. *Engineering Fracture Mechanics, 127*, 97-103.

Steinbrunner, D. L., Matlock, D., & Krauss, G. (1988). Void formation during tensile testing of dual phase steels. *Metallurgical transactions A, 19*(3), 579-589.

Sun, S., & Pugh, M. (2002). Properties of thermomechanically processed dual-phase steels containing fibrous martensite. *Materials Science and Engineering: A, 335*(1-2), 298-308.

Szewczyk, A., & Gurland, J. (1982). A study of the deformation and fracture of a dual-phase steel. *Metallurgical transactions A, 13*(10), 1821-1826.

Vajragupta, N., Uthaisangsuk, V., Schmaling, B., Münstermann, S., Hartmaier, A., & Bleck, W. (2012). A micromechanical damage simulation of dual phase steels using XFEM. *Computational Materials Science, 54*, 271-279.

Wu, B., Vajragupta, N., Lian, J., Hangen, U., Wechsuwanmanee, P., & Münstermann, S. (2017). Prediction of plasticity and damage initiation behaviour of C45E+ N steel by micromechanical modelling. *Materials & Design, 121*, 154-166.